Filamentation with Ultra Short Pulse in Air and its applications

N. Nuntawong and J. Yeak

University of New Mexico

Abstract. We report here the recent progresses in both theoretical and experimental studies on the propagation of ultra short optical high-energy pulse through the atmosphere. The applications based on promising properties of long filamentation in air have been presented. These include white light LIDAR and laser lightning control.

INTRODUCTION

Self-focusing of light is the process in which index of refraction of material is modified by intense beam of laser in such a manner that leads to a focus within material, which is typically known as Kerr-lens effect. At a certain condition when the power in the laser beam exceeds a critical power, the intensity dependent refractive index will lead to a nonlinear curvature of the laser wavefront, which overcomes the effect of linear diffraction and produce moving focus of the beam [1-3]. This can give the perception of a self-focused beam moving along the propagation axis. As the intensity becomes very high closer to the self-focusing point, this will lead to high-order production of plasma along the laser beam propagation. Even after the laser pulse has disappeared, it will leave behind a plasma column. This plasma column is often referred as a plasma filament while the laser pulse referred as an optical filament as shown in Figure 1.

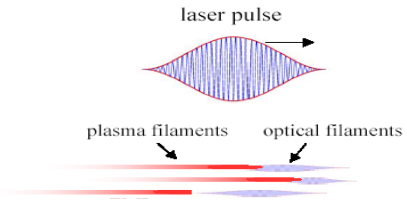

Figure 1: Schematic show laser beam filamentation component. AfterRef.[4]

The properties of laser beam filamentation in air open exciting perspectives for application such as white-light light detection and ranging (LIDAR) and laser lightning control, and the recent progress of these applications will be presented in this report. These applications need a sufficient characterization of the filament formation over atmospheric scale such as in km range.

The filament onset and length are important parameters for spectroscopic measurement of atmospheric components, which require depositing energy at a long distance target. The application of filamentation for remote sensing in atmosphere is extremely important for understanding global warming, ozone loss and weather models [5]. The laser lightning control is also an interesting research tool to help understand the mechanism of lightning. It may offer innovative possibilities for active protection of sensitive installations such as strategic sites, including nuclear, biological, and chemical plants.

THEORY

We know that once the beam power exceeds the critical power, $P_{cr} = \lambda^2/(8\pi n_0 n_2)$, the beam start to self-focus to a point. However, the catastrophic collapse is negated due to the ionization of air creating a plasma which in turn defocuses the beam. A self-induced waveguide in air or better known as a filament occurs when a dynamic balance between self-focusing, plasma defocusing and diffraction is met. Recent experiments have shown that this self-guided pulse propagates over many Rayleigh lengths with a diameter on the order of around 100 μm [7-9].

Most research work on filaments has mainly been confined to the near infrared wavelengths (around 800nm) simply because of the relatively ease in obtaining ultrashort pulses (down to 30 fs) with Ti:Sapphire chirped pulse laser system. Since the critical power at 800nm is about 2 GW, about 65 times higher (due to a much lower n_2 in the near infrared regime), more nonlinear phenomena are involved compared to UV wavelengths. For example, the acceleration of electrons due to inverse Bremsstrahlung that leads to cascade ionization in the formation of the plasma happens in subpicosecond time scale, higher peak powers are required for filamentation. Consequently, higher order dispersion terms come into play. Besides, one has to also question the validity of using the slowly varying envelope approximation (SVEA) when using ultrashort pulses of down to a few optical cycles to meet the condition for filamentation [10]. There is an active on-going research in modeling ultrashort pulse propagating in air [11-13].

A modified nonlinear envelope equation can be used to include the effects of multiphoton absorption (MPA) and plasma formation in the modeling of ultrashort pulse propagation [11]. Assume the pulse propagates along the z-axis and has radial symmetry with a wave vector $k = n_0\omega_l/c$, where n_0 is the linear refractive index and ω_l is the central frequency of the laser pulse. Let the input pulse at $z = 0$ to be Gaussian in space and time such that $E(r,z=0,t) = E_0 exp[-r^2/2w_0^2 - t^2/2\tau_p^2]$. Normalizing the amplitude $u(r,z,t) = E(r,z,t)/E_0$, and using the normalized retarded time frame $\tau = (t-z/v_g)/\tau_p$, we obtain

$$\frac{\partial u}{\partial \zeta} = \frac{i}{4}\left(1+\frac{i}{\omega_l \tau_p}\frac{\partial}{\partial \tau}\right)^{-1} \nabla_\perp^2 u - i\frac{L_{df}}{L_{ds}}\frac{\partial^2 u}{\partial \tau^2} + i\left(1+\frac{i}{\omega_l \tau_p}\frac{\partial}{\partial \tau}\right)P^{NL} \quad (1)$$

where $L_{df} = kw_0^2/2$ is the diffraction length, $\zeta = z/L_{df}$ is the normalized distance, $L_{ds} = \tau_p^2/\beta_2$ is the dispersion length, β_2 is the group velocity disperson and P^{NL} is the normalized nonlinear polarization. We can incorporate all nonlinear terms in P^{NL} that include the effects of the nonlinear refractive index change, multiphoton absorption and formation of electron plasma. If we neglect the nonlinear polarization source term in Equation (1), we see that the term $(1+i\partial/\omega_1\tau_p\partial\tau)$ gives rise to space-time focusing and self-steepening effects (or known as "optical shock"). These effects are responsible for the asymmetrical broadening of spectrum as shown in Figure 2. The optical shock term here gives rise to the supercontinuum generation (or white light) that is often associated with filamentation. This property of filaments is fully utilized by researchers in LIDAR applications [5,14,15].

Solving Equation (1) can be very difficult since we are looking at changes in the beam size on the order of tens of microns and pulsewidths of femtosecond time scale over tens of meters of propagation. However, the on-going research work at UNM has mainly been revolving around UV filaments due to the less stringent requirement for P_{cr} [16,17]. Since the P_{cr} is much lower (on the order of 30 MW) in this regime, filaments can be formed by using longer pulses. In this approximation, we are able to use SVEA in solving Maxwell's equations.

We know from Maxwell's equations, pulse propagation in air obeys

$$\left(\frac{\partial^2}{\partial x^2}+\frac{\partial^2}{\partial y^2}+\frac{\partial^2}{\partial z^2}-\frac{1}{c^2}\frac{\partial^2}{\partial t^2}\right)E(x,y,z,t)=\mu_0\frac{\partial^2}{\partial t^2}P(x,y,z,t) \quad (2)$$

with $P = P^L + P^{NL}$ consists of the linear and nonlinear polarization of air. The generation of plasma and other nonlinear phenomena can be considered as higher order terms in the expression of the refractive index of air as given [18]

$$n = n_0 + n_2 I + n_m I_m^{m/2} \quad (3)$$

with m being greater than 2 (due to the higher order dispersion terms involved). Thus, we can write the susceptibility associated with the refractive index as

$$P^{NL} = \varepsilon_0\left[\chi^{(3)}\left|\tilde{\mathrm{E}}\right|^2 + \chi^{(m+1)}\left|\tilde{\mathrm{E}}\right|^m\right]E \quad (3)$$

$$\text{with } \chi^{(m+1)} = 2n_0\left(\frac{\varepsilon_0 c n_0 n_m}{2}\right) = \varepsilon_0 c n_0^2 n_m \quad (4)$$

$$\text{and } E = \tilde{E}e^{i(\omega_1 t - kz)} \quad (5)$$

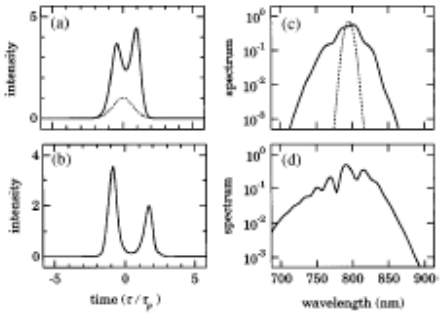

Figure 2: Theoretical predictions of the temporal intensity profile (a) and (c), and the power spectra (b) and (d) of the transmitted beam. The dashed line in (a) and (b) represents the temporal profile and spectrum of the input pulse. In (a) and (b), the input power is 1.75 P_{cr} and in (c) and (d) 1.9 P_{cr} (After Ref. 10)

The lowest order correction to the expansion of the nonlinear index is cubic term in the electric field,

$$P^{NL} = \varepsilon_0\left[\chi^{(3)}\left|\tilde{\mathrm{E}}\right|^2 + \chi^{(4)}\left|\tilde{\mathrm{E}}\right|^3\right]\tilde{E}e^{i(\omega t-kz)} \quad (6)$$

This leads to a modified nonlinear Schrodinger equation:

$$\left[\frac{\partial}{\partial z}+\frac{i}{2k}\left(\frac{\partial^2}{\partial x^2}+\frac{\partial^2}{\partial y^2}\right)-\frac{ik}{2}\left(\chi^{(3)}\left|\tilde{\mathrm{E}}\right|^2+\chi^{(4)}\left|\tilde{\mathrm{E}}\right|^3\right)-\alpha\right]\tilde{E}=0 \quad (7)$$

with α is the linear gain or absorption associated with the imaginary part of linear index of refraction. Assuming a Gaussian shape for the field envelope in cylindrical coordinates,

$$\mathrm{E}(z,r)=\frac{w_0}{w}\mathrm{E}_0 e^{-\frac{r^2}{w^2}}e^{-i\frac{kr^2}{2R}-i\varphi} \quad (8)$$

Equation (12) becomes, assuming negligible attenuation,

$$\frac{d^2w}{dz^2}=-\frac{4}{k^2}\left(\frac{P}{P_{cr}}-1\right)\frac{1}{w^3}+a\frac{1}{w^4}P^{\frac{3}{2}} \quad (9)$$

$$\text{and } \frac{1}{P}\frac{dP}{dz}=-\beta_3\frac{1}{w^4}P^2-\beta_4\frac{1}{w^3}P^{\frac{3}{2}} \quad (10)$$

where Equation (9) describes the beam size variation and Equation (10) the beam power along the propagation distance z. Equations (9) and (10) can be integrated analytically to give

$$\left(\frac{dw}{dz}\right)^2=\frac{4}{k^2}\left[\frac{P}{P_{cr}}-1\right]\left[\frac{1}{w^2}-\frac{1}{w_0^2}\right]-\frac{4l}{n_0}\beta_4\left[\frac{1}{w^3}-\frac{1}{w_0^3}\right]P^{\frac{3}{2}}+\frac{w_0^2}{R_0^2} \quad (11)$$

$$\text{with } \beta_3=\left(\frac{2}{\pi}\right)^2\beta_{MPI}=\left(\frac{2}{\pi}\right)^2 3\hbar\omega_1 N_0\sigma^{(3)}$$

$$\beta_4=-\left(\frac{2}{\pi}\right)^{\frac{3}{2}}\frac{n_3}{l},\ a=\left(\frac{6l}{n_0}\right)\beta_4 \text{ and } l=c/(2\upsilon_{ep})$$

where β_3 is the three-photon power absorption, β_4 the plasma nonlinear power absorption and l the mean free path length of electrons in the plasma. From Equation (14), the first term on the left corresponds to self-focusing above critical power, the second term due to the linear diffraction of the beam, and the third term self-defocusing of the plasma. The physical interpretation of Equation (11) is given by Figure 3 showing the filamentation process where self-focusing increases the electron density of the plasma which in turn defocuses the beam.

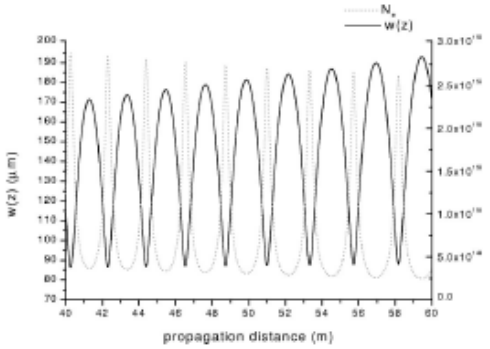

Figure 3: Beam size w and electron density Ne versus propagation distance with initial power of 49.5 MW. (After Ref. 17).

Equations (9)-(11) do not indicate any generation of white light accompanying the filamentation process. This is in agreement with Equation (1) proposed by Gaeta that there is no spectrum broadening for *m* greater than 3. Since there is no associated loss due to white light, UV filaments should propagate over much longer distances than IR filaments. As can be seen in Figure 4, light can be trapped within filaments of the order of 100 μm over 100m of propagation distance. This opens up the prospects of triggering and guiding lightning discharges with filaments over long distances.

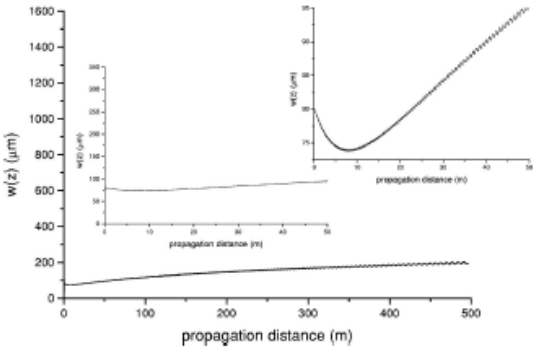

Figure 4: Beam size w versus distance for an initial power of 160MW (After Ref. 17)

FILAMENTATION IN AIR AND WHITE LIGHT GENERATION

Recent studies of self-focusing of ultrashort laser pulses in air have demonstrated a level of extended complexity for light pulses shorter than a picosecond at a power larger than P_{cr}. As a result due to a dynamic balance between Kerr-lens focusing and defocusing on laser-induced plasma, a breakup of the beam into one or several filaments [14] of about 100 μm in diameter that propagate over distances much longer than the Rayleigh length. Each filament contains a very high intensity of typically 10^{14} W/cm^2. At this very high power, which allows efficient self-phase modulation, an "optical shock" forms at the rear edge of pulse [9], resulting in the emission of a broadband white-light spectrum spanning from the UV to the mid-IR [9] which is known as super continuum generation (SCG) [19]. An excellent example of filamentation in air is the observation of long-distance white light propagation as shown in Figure 5. This phenomenon was first observed with 100-fs laser pulse in the near infrared [6, 12] with the initial energy above 10 mJ, which produce light filament with a diameter of 100 μm and a length of several meters. At higher initial powers, the beam exhibit pulse spliting, multiple collapse [20], and repeated filamentation [21]. Figure 6 demonstrate that the spectrum of super continuum or white-light generation extends from the UV to the mid-infrared up to 4 μm, which covers the absorption bands of many important pollutants, such as volatile organic compounds (VOCs).

Wille et al. [15] have shown that the onset of filamentation strongly depends on the peak power and initial chirp. Negatively chirp pulse (i.e., launching the blue part of the spectrum before the red part) can be used to compensate group-velocity dispersion (GVD) in air, and thus to select the distance at which the Fourier components will recombine, leading to white-light generation. With an adequate group velocity dispersion (GVD) precompensation, filamentation altitude can be extended to greater than 10 km into the atmosphere [14].

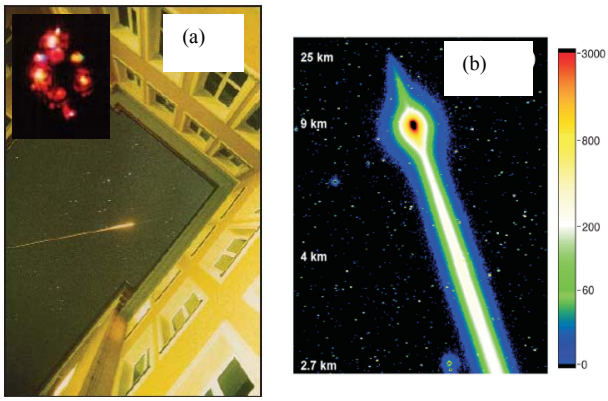

Figure 5: Light filamentation in air. (a) Photograph of a terawatt femtosecond laser pulse directed into the sky from the University of Jena (inset).Photograph of the beam at a point transverse to the propagation direction shows multiple filaments and white light emission from each of filaments. After Ref.[5]. (b) The white light from filaments can extend more than 10 km into the atmosphere.[14]

Figure 7 shows the effect of different GVD precompensation on the filamentation attitude taken from ref.[11]. In the first case (a), the near-infrared (800 nm) beam with the peak power of 3 TW is sent with a very low GVD compensation (corresponding to an initial duration of 150 fs of the launched pulse). The profile images have been taken on a cloud at 6 km altitude. The observed images on the cloud exhibit a ring structure with a diameter of 32 m. This ring is clearly the projection of conical emission from the filaments formed at lower altitudes. In this case, the ring structure on the cloud leads to an half angle from ground of about 2.7 mrad, which is typical for the angle of conical emission in this spectral region [22].

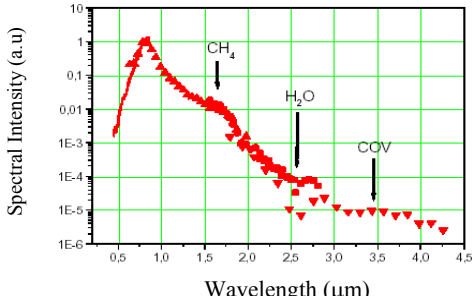

Figure 6: Spectrum of the white-light continuum produced by an ultrashort laser pulse in the air [20]

Thiis indicates that the filaments are generated (and end) close to the ground level as shown in Figure 7(a). In another case, the laser beam of same wavelength but with an initial negative chirp corresponding to 600 fs pulse duration to compensate GVD has

been sent. In this case, the narrow ring merges to the central peak. Considering that the initial chirp of the pulse does not affect the angle of conical emission [22]. The reduced projected radius of conical emission is the signature for an emission occurring nearer the cloud. In this particular experiment, the filament altitude shown in Figure 7(b) has been calculated to be about 2km.

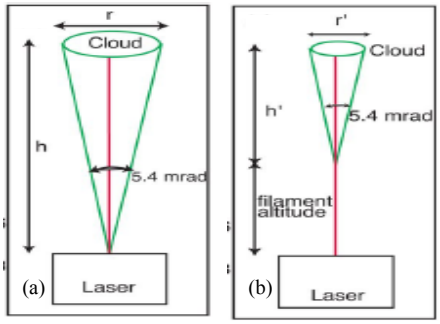

Figure 7: (a) Schemetic of the ring emitted from low-altitude filaments imaged on high-altitude cloud. (b) for a stronger GVD precompensation, pushing the filamentation to higher altitudes, and reducing the apparent diameter of the imaged conical emission..

WHITE LIGHT LIDAR

The classical techniques of remote sensing of the atmosphere such as balloon and aircraft borne instrument are capable to obtain the variety of data. However, those local methods can be very expensive for routine daily studies. The other main techniques are use of optical techniques such as Fourier transform spectroscopy (FTIR) and differential optical absorption spectroscopy (DOAS). However, these two methods detect the absorption the Sun or Moon as light sources, which are limited by intensity and predetermined absorption path [9, 23]. In contrast, LIDAR is based on atmospheric backscatter signal from actively emitted light pulse which can eliminate those limits and provides 3-D distributions of atmospheric constituents.

The remote white light source for remote sensing can be achieved by generating a laser induced plasma focus in atmosphere with an appropriate compensated group-velocity dispersion (GVD) as discussed above.

An example of fs-LIDAR experimental setup utilizing remote white-light generation and filamentation altitude control discussed above is shown in Figure 8(a). After passing a (negative) chirp generator, the fs-laser pulses are launched into the atmosphere. As a result, filaments are generated at a predetermined distance. The backscattered white light is then collected by a telescope and focused through a spectrometer on a time-resolved detector. Figure 8(b) shows three transients of spectrally filtered return signals recorded in the time window after the laser pulse was launched. The vertical axis indicated the altitude at which the signals were backscattered. The initially strong signal increase is due to the progressive overlap between laser and telescope field of view. The white-light signal at 600 nm reaches an altitude of > 5 km. Stronger Rayleigh scattering at shorter wavelengths causes the UV wavelength to vanish shortly above 1 km.

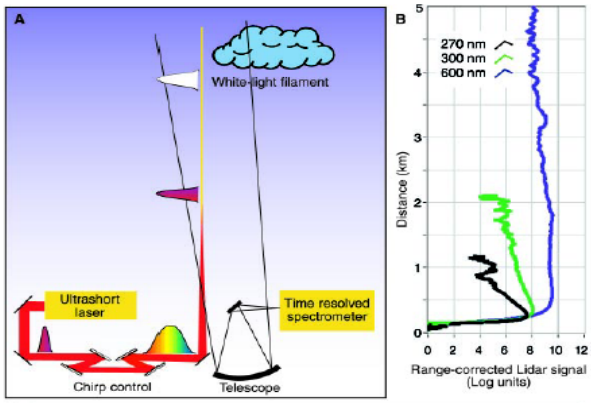

Figure 8: (a) Schemetic of fs-LIDAR experimental setup. (b) Vertical white-light LIDAR profile at three different wavelength .After Ref.[6]

The ability to perform high-resolution measurements over a wide spectral range using white-light LIDAR is illustrated in Fig.9. The measurement was recorded at an altitude of 4.5 km. It presents the highly resolved optical fingerprints of the atmosphere along a very long absorption path. White-light LIDAR might also simultaneously yield wind profiles through the measurement the measurement of Doppler shift. Recently, analysis of droplet size distribution and density using white-light LIDAR technique has been reported [24]. Although preliminary, it open the new way to precipitation forecast.

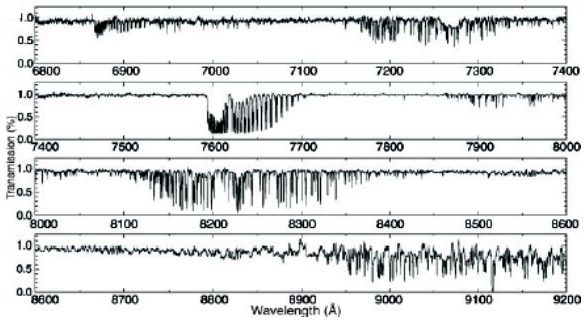

Figure 9: High-resolution atmospheric absorption spectrum from an altitude of 4.5 km. After Ref.[9]

LASER LIGHTNING CONTROL

The potential of lasers to manipulate the path of lightning has been discussed since the 1970s [25]. The early studies using nanosecond lasers exhibited severe limitations due to the lack of connected plasma channels. However, the advent of high-power femtosecond lasers has opened new perspective in this research.

The work done by J.-C. Diels here at UNM pioneered the work in laser-triggered and –guided lightning with fs UV lasers [26]. Recent work by the Teramobile group in Europe demonstrated that a high voltage of 2MV was discharged in a well-guided way up to 3 m as shown in Figure 10 [27]. The Teramobile system of wavelength at 790 nm was placed inside the high-voltage facility of the Technical University of Berlin, with its horizontal output beam in line with the electrodes. The filament spanned the whole 1- to 3-m gap between the electrodes as shown in Figure 10(a). The typical erratic discharge between the two electrodes, when no laser is present, is shown in Figure 10(b). The breakdown voltage was reduced by 33% with IR filaments, demonstating the ability of fs-filaments to trigger high-voltage discharge by ohmic bridging of the electrodes.

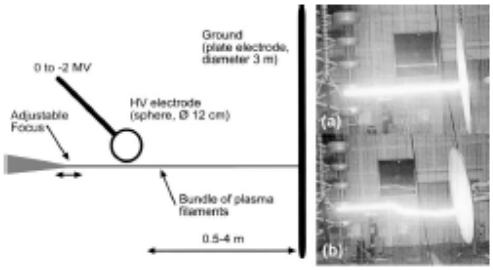

Figure 10: Experimental setup and results of the HV discharge at Berlin in the TERAMOBILE Project

La Fontaine et al.,[28] have demonstrate the difference in the velocity of natural discharge and that of a laser-guide discharge with IR filaments as illustrated in Figure 11. Over the first meter of charge propagation, the velocity of laser-guided discharge is between five and ten times that of the natural discharge. This is

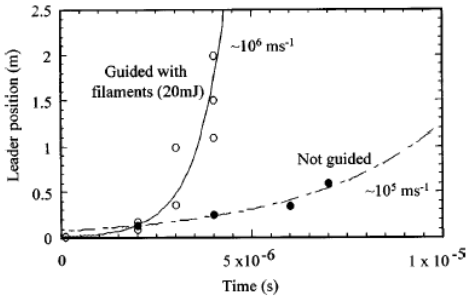

Figure 11. Evolution of the position of discharge inside the gap. Afte Ref.[28]

due to the present of free charges inside the filament that supports the charge flow. Studying of high voltage discharges with UV filaments is currently underway at UNM .

CONCLUSION

In the past decade, knowledge about the filamentation formed by ultrashort laser pulses in air and the related nonlinear optical effect has progressed steadily. The effect of filamentation in air such as remote white-light generation is very promising for application in atmospheric science. This includes remote analysis of the atmosphere in the field of multicomponent trace-gas diagnosis by fs white-light LIDAR. Several experiments of laser lighting control have raised hopes for application to protect sensitive site from natural lighting. The development of these applications will further be assisted by the progress in ultrafast laser technology.

REFERENCES

[1] M. Mlejnek, E.M. Wright, J.V. Moloney, IEEE J. Quantum Electronics, **35**, 12, pp. 1771-1776 (1999).

[2] A. L. Gaeta, Science. **301,** 54 (2003).

[3] A. Brodeur, C. Y. Chien, F.A. Ilkov, S. L. Chin, O. G. Kosareva, and V. P. Kandidov, Opt. Lett. **22,** 304 (1997).

[4] J. Penano, NTAR Symposium. (2004).

[5] J. Kasparian et. al., Science. **301,** 61 (2003).

[6] R. Ackermann, Appl. Phys. Lett. **85**, 5781 (2004).

[7] A. Braun et al., Opt. Lett. **20**, 73 1995).

[8] E.T.J. Nibbering et al., Opt. Lett. **21**, 62 (1996).

[9] J. Kasparian, et al., Opt. **25**, 18 (2000).

[10] J.K. Ranka, A.L. Gaeta, Opt. Lett. **23**, 7, 1998.

[11] A. L. Gaeta, Phy. Rev. Lett. **84**, 3582 (2000).

[12] T. Brabec, F. Krausz, Phys. Rev. Lett. **78**, 12, 3282 (1997).

[13] M. Kolesik, M. Mlejnek, J.V.Moloney, Phys. Rev. Lett.**89**, 28 (2002).

[14] P. Rairoux et al., Appl. Phys. B. B **71**, 573 (2000).

[15] H. Wille, M. Rodriguez, J. Kasparian, D. Mondelain, J. Yu, A. Mysyrowicz, R. Sauerbrey, J. –P Wolf, and L. Woste, Eur. Phys. J.: Appl. Phys. **20**, 183 (2002).

[16] J. Schwarz, et al., Opt. Comm. **180**, 383 (2000).

[17] J. Schwarz, J.-C. Diels, Phys. Rev. A. **65**, 013806 (2001).

[18] J.-C. Diels, W.Rudolph, Ultrashort Laser Pulse Phenomena, Academic Press, 2nd Edition.

[19] R. R. Alfano, Ed., The Super Continuum Laser Source (Springer, New York, 1989).

[20] A. Talebpour, S. Petit and S. L. Chin, Opt. Commun. **171**, 285 (1999)

[21] S. Tzortzakis et al., Phys. Rev. Lett.**86**, 5470 (2001).

[22] O. G. Kosareva, V. P. Kandidov, A. Brodeur, C. Y. Chen, and S. L. Chin, Opt. Lett. **22**, 1332 (1997)

[23] R. A. Meyers, Ed., Encyclopedia of analytical Chemistry (Wiley, Chichester, UK, 2000), Vol.3.

[24] R. Bourayou et al, J. Opt. Soc. Am. B. **22**, 369(2005).

[25] D. W. Koopman and T. D. Wilkerson, J. Appl. Phys. **42**, 1883 (1971).

[26] X.M.Zhao et al., IEEE J. Quantum Electron. **31**, 599 (1995).

[27] M. Rodriguez, et al. Opt. Lett. **27**, 9 (2002).

[28] B. L. Fontaine et al, J. Appl. Phys. **88**, 610(2000)